

# Isotopic effects in multifragmentation and the nuclear equation of state

W. Trautmann<sup>a</sup> and the ALADIN and INDRA collaborations

<sup>a</sup>Gesellschaft für Schwerionenforschung mbH,  
D-64291 Darmstadt, Germany

Isotopic effects in spectator fragmentations following heavy-ion collisions at relativistic energies are investigated using data from recent exclusive experiments with SIS beams at GSI. Reactions of  $^{12}\text{C}$  on  $^{112,124}\text{Sn}$  at incident energies 300 and 600 MeV per nucleon were studied with the INDRA multidetector while the fragmentation of stable  $^{124}\text{Sn}$  and radioactive  $^{107}\text{Sn}$  and  $^{124}\text{La}$  projectiles was studied with the ALADIN spectrometer.

The global characteristics of the reactions are very similar. This includes the rise and fall of fragment production and deduced observables as, e.g., the breakup temperature obtained from double ratios of isotope yields. The mass distributions depend strongly on the neutron-to-proton ratio of the decaying system, as expected for a simultaneous statistical breakup. The ratios of light-isotope yields from neutron-rich and neutron-poor systems follow the law of isoscaling. The deduced scaling parameters decrease strongly with increasing centrality to values smaller than 50% of those obtained for the peripheral event groups. This is not compensated by an equivalent rise of the breakup temperatures which suggests a reduction of the symmetry term required in a liquid-drop description of the fragments at freeze-out.

## 1. INTRODUCTION

Two themes are presently prevailing in the discussion of nuclear multifragmentation. One of them concerns the order of the nuclear liquid-gas phase transition. It should be of first order according to the range dependence of the nuclear forces but phenomena characteristic of second-order transitions are equally present in multifragmentation data [ 1, 2, 3]. The second class of questions is related to the nuclear equation of state and to its importance for astrophysical processes. Supernova simulations or neutron star models require inputs for the nuclear equation of state at extreme values of density and asymmetry for which the predictions differ widely [ 4, 5]. Fragmentation reactions are of interest here because they permit the production of nuclear systems with subnuclear densities and temperatures which, e.g., largely overlap with those expected for the explosion stages of core-collapse supernovae [ 6]. Laboratory studies of the properties of nuclear matter in the hot environment, similar to the astrophysical situation, are thus becoming feasible, and an active search for suitable observables is presently underway. Of particular interest is the density-dependent strength of the symmetry term which is essential for the description of neutron-rich objects up to the extremes encountered in neutron stars (refs. [ 7, 8, 9] and contributions to this conference).

Here, new results from two recent experiments performed at the GSI laboratory will be discussed with particular emphasis on the second class of topics. The INDRA multidetector [ 10] has been used to study isotopic effects in nearly symmetric  $^{124,129}\text{Xe}$  on  $^{112,124}\text{Sn}$  reactions at incident energies up to 150 MeV per nucleon and spectator fragmentations in  $^{12}\text{C}$  on  $^{112,124}\text{Sn}$  at incident energies 300 and 600 MeV per nucleon. In a very recent experiment with the ALADIN spectrometer, the possibility of using secondary beams for reaction studies at relativistic energies has been explored. Beams of  $^{107}\text{Sn}$ ,  $^{124}\text{Sn}$ ,  $^{124}\text{La}$ , and  $^{197}\text{Au}$  as well as Sn and Au targets were used to investigate the mass and isospin dependence of projectile fragmentation at 600 MeV per nucleon. The neutron-poor radioactive projectiles  $^{107}\text{Sn}$  and  $^{124}\text{La}$  were produced at the Fragment Separator FRS by fragmentation of a primary beam of  $^{142}\text{Nd}$  and delivered to the ALADIN experiment.

The data analysis performed so far includes isotopic effects in neutron and fragment production, isoscaling and its relation to the properties of hot fragments at the low-density freeze-out, flow in mass-symmetric collisions at intermediate energy, transparency in central collisions at intermediate energies as obtained from isospin tracing, as well as size fluctuations of the heaviest fragment of the partition and their relation to the order of the phase transition [ 2]. In the following, emphasis will be given to phenomena encountered in spectator fragmentation which is believed to occur at low density in the region of liquid-gas coexistence of the nuclear-matter phase diagram.

## 2. THE PHASE DIAGRAM

A phase diagram of nuclear matter as it is of interest in multifragmentation has been discussed some years ago at a previous conference of this series (Fig. 1, bottom left, from ref. [ 11]). It is partly schematic, with the boundary of coexistence (CE) and the adiabatic spinodal (AS) adapted from ref. [ 12], and partly theoretical, with critical points as derived for nuclear matter [ 12, 13] and for a  $^{16}\text{O}$  nucleus in a container [ 14]. The three experimental points representing the freeze-out conditions in spectator fragmentation were obtained by correlating results from temperature measurements and from interferometry performed in ALADIN experiments [ 15, 16].

In more recent years, the established systematics of freeze-out temperatures [ 17] and alternative indications for the expansion prior to freeze-out [ 18, 19] have confirmed this general picture. Freeze-out occurs in the coexistence zone below the critical temperature and at densities equivalent to a fraction of the normal nuclear density. New evidence has also been obtained for the equilibrium nature of the freeze-out configurations. For example, the systematics of fragment multiplicity versus excitation energy compiled by Tamain [ 20] shows that multifragmentation is a universal phenomenon driven by the thermal excitation of the system, fairly independent of the type of collision through which it is imparted. The achievement of equilibrium is important for the astrophysical implications as the time scales encountered there are slow, corresponding to equilibrium situations on the nuclear scale.

## 3. GROSS PROPERTIES

Isotopic effects are rather small for global observables of the studied reactions as, e.g., the multiplicity of the produced intermediate-mass fragments or the correlation of the

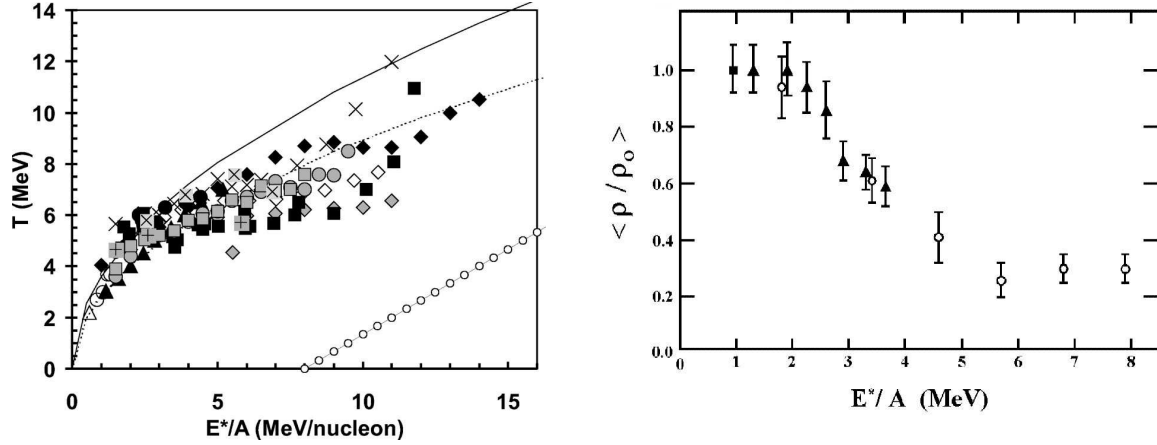
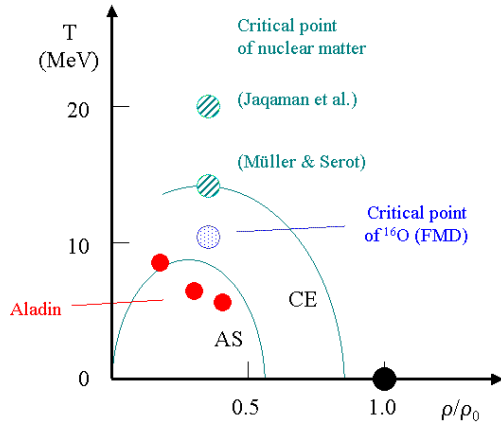


Figure 1. Left: temperature-versus-density diagram with the saturation point of nuclei (closed circle), calculated critical points of nuclear matter (hatched), the critical temperature of  $^{16}\text{O}$  according to the FMD model and with experimental results (dots) obtained by correlating measured temperatures and densities (from ref. [ 11]).



Top panels: temperatures (left) and densities (right) of fragmenting systems at the freeze-out stage as a function of their excitation energy per nucleon. For details see refs. [ 17, 18, 19].

maximum charge  $Z_{\text{max}}$  with  $Z_{\text{bound}} = \sum Z_i$  with  $Z_i \geq 2$  (Fig. 2; the sorting variable  $Z_{\text{bound}}$  is related to the impact parameter and inversely related with the excitation energy per nucleon of the produced spectator system). The universal rise and fall of fragment production [ 21] is recovered (Fig. 2, left panel) and only a slightly steeper slope in the rise section distinguishes the neutron-rich case of  $^{124}\text{Sn}$  from the other two systems. As confirmed by statistical model calculations [ 22], this difference is related to the evaporation properties of excited heavy nuclei. Neutron emission prevails for neutron-rich nuclei which leads to a concentration of the residue channels, with small associated fragment multiplicities, in a somewhat narrower range of large  $Z_{\text{bound}}$  than in the neutron-poor cases exhibiting stronger charged-particle emissions. The evaporation of protons reduces  $Z_{\text{bound}}$  since protons are not counted therein.

The effect is, nevertheless, small and nearly invisible in the correlation of  $\langle Z_{\text{max}} \rangle$  with  $Z_{\text{bound}}$  (Fig. 2, right panel). In this correlation the transition from predominantly residue production to multifragmentation becomes apparent as a reduction of  $\langle Z_{\text{max}} \rangle$  with respect to  $Z_{\text{bound}}$ , approximately representing the total charge of the decaying system, which occurs at  $Z_{\text{bound}}/Z_{\text{proj}} = 0.7$  to  $0.8$ . Small differences are also observed for the fragment  $Z$  spectra [ 2] and for deduced quantities as, e.g., the breakup temperature obtained from double ratios of isotope yields discussed below. The range of isotopic compositions

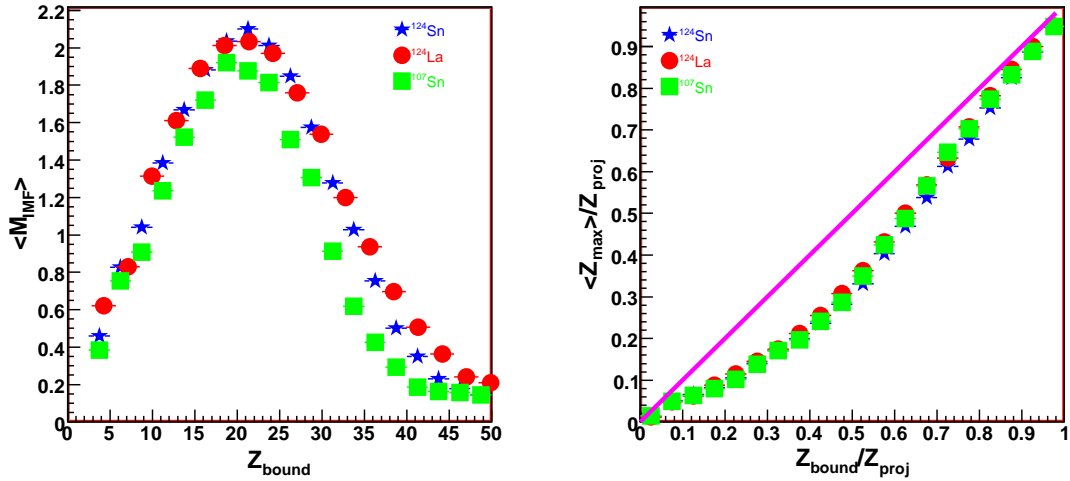


Figure 2. Mean multiplicity  $\langle M_{\text{IMF}} \rangle$  of intermediate-mass fragments  $3 \leq Z \leq 20$  produced in the fragmentation of  $^{107,124}\text{Sn}$  and  $^{124}\text{La}$  (600 A MeV, ALADIN) as a function of  $Z_{\text{bound}}$  (left panel). The right panel shows the correlation of the mean  $Z$  of the largest fragment with  $Z_{\text{bound}}$  with both quantities normalized with respect to the projectile  $Z$ .

of the studied nuclei  $N/Z = 1.14$  to  $1.48$  is not sufficiently large, so that significant variations of the reaction mechanism would appear. A shrinking of the coexistence zone in the temperature-density plane is expected for neutron-rich matter but larger consequences can only be expected for asymmetries far beyond those presently available for laboratory studies [12]. This fact, on the other hand, has the important consequence that the basic reaction process is the same for all the studied cases, a prerequisite for the interpretation of isoscaling and its relation with the symmetry energy.

#### 4. ISOTOPIC EFFECTS IN LIGHT FRAGMENT PRODUCTION

The mass resolution obtained for projectile fragments entering into the acceptance of the ALADIN spectrometer is about 3% for fragments with  $Z = 3$  and decreases to 1.5% for  $Z \geq 6$ . Masses are thus individually resolved for fragments with atomic number  $Z \leq 10$ . The elements are resolved over the full range of atomic numbers up to the projectile  $Z$  with a resolution of  $\Delta Z \leq 0.2$  obtained with the TP-MUSIC IV detector [22].

The mean  $N/Z$  of the inclusive isotope distributions of light fragments in the range  $3 \leq Z \leq 9$  is presented in Fig. 3. The values for  $Z = 4$  have been corrected for the missing yield of unstable  $^8\text{Be}$  by including an estimate for it obtained from a smooth interpolation over the identified yields of  $^{7,9-11}\text{Be}$ . This correction has a negligible effect for the case of  $^{107}\text{Sn}$  but lowers the  $\langle N \rangle / Z$  of Be for  $^{124}\text{Sn}$  from 1.24 to 1.18 which makes the systematic odd-even variation more clearly visible for the neutron rich case. The odd-even staggering is more strongly pronounced for the neutron-poor  $^{107}\text{Sn}$ . The strongly bound even-even nuclei attract a large fraction of the product yields during the secondary evaporation stage [23]. Their effect is, apparently, larger if the hot fragments are already close to symmetry, as it is expected for the fragmentation of  $^{107}\text{Sn}$  [24].

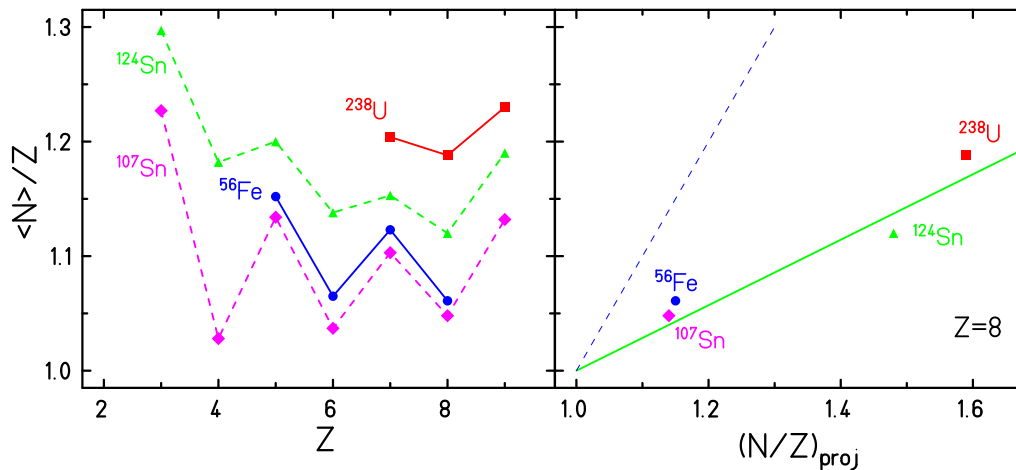


Figure 3. Inclusive mean values  $\langle N \rangle / Z$  of light fragments with  $3 \leq Z \leq 9$  produced in the fragmentation of  $^{107,124}\text{Sn}$  (600 A MeV, ALADIN),  $^{56}\text{Fe}$  and  $^{238}\text{U}$  (both 1 A GeV, FRS) as a function of the fragment  $Z$  (left panel). The right panel shows the results for  $Z = 8$  as a function of the  $N/Z$  value of the projectile. The lines represent the trend of the data (full line) and  $\langle N \rangle / Z = (N/Z)_{\text{proj}}$  (dashed).

Inclusive data obtained with the FRS fragment separator at GSI for  $^{238}\text{U}$  [ 23] and  $^{56}\text{Fe}$  [ 25] fragmentations on titanium targets at 1 A GeV bombarding energy confirm that the observed patterns are very systematic, exhibiting at the same time nuclear structure effects characteristic for the isotopes produced and significant memory effects of the isotopic composition of the excited system by which they are emitted. This has the consequence that, because of its strong variation with  $Z$ , the neutron-to-proton ratio  $\langle N \rangle / Z$  is not a useful observable for studying nuclear matter properties. For this purpose, techniques, such as the isoscaling discussed below, will have to be used which cause the nuclear structure effects to cancel out. Selecting a particular element, e.g.  $Z = 8$ , is already sufficient to reveal the clear correlation of  $\langle N \rangle / Z$  with the  $N/Z$  of the projectile (Fig. 3, right panel). According to the Statistical Fragmentation Model (SMM, ref. [ 26]), the correlation should be much stronger for the hot fragments of the breakup stage and, in fact, not deviate much from the dashed  $\langle N \rangle / Z = (N/Z)_{\text{proj}}$  line in the figure [ 24]. The difference is due to sequential decay and its being directed toward the valley of stability. A precise modeling of these secondary processes is, therefore, necessary for quantitative analyses.

## 5. ISOSCALING

The experimental study of particle and fragment production with isotopic resolution has led to the identification of isoscaling, a phenomenon shown to be common to many different types of heavy-ion reactions [ 27, 28, 29, 30]. It is observed by comparing product yields  $Y_i$  from reactions which differ only in the isotopic composition of the projectiles or targets or both. Isoscaling refers to an exponential dependence of the measured yield ratios  $R_{21}(N, Z)$  on the neutron number  $N$  and proton number  $Z$  of the detected products.

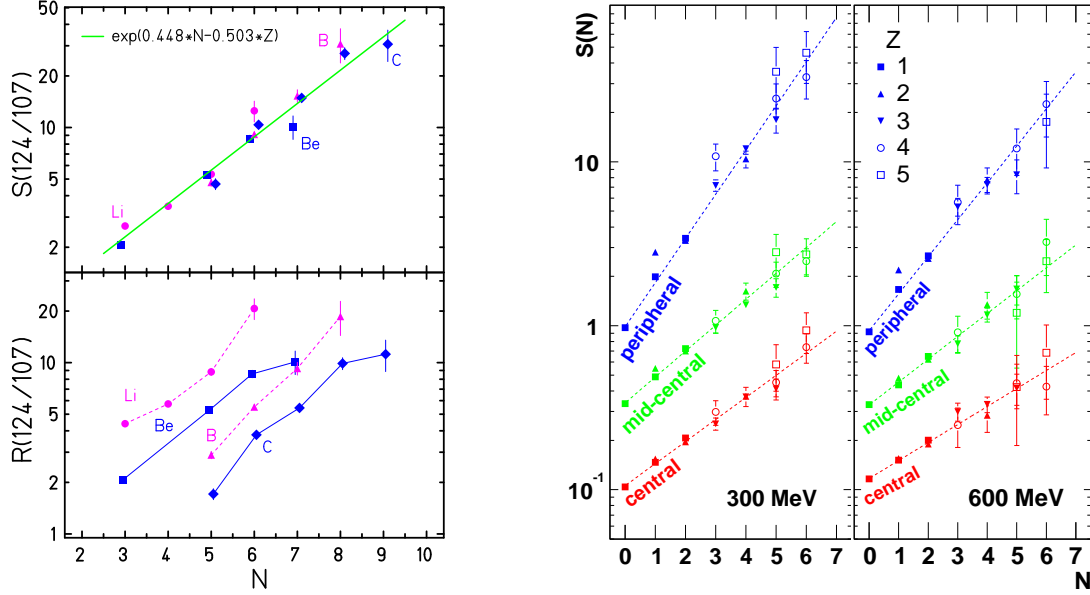


Figure 4. Left panels: Normalized yield ratios  $R(N)$  (bottom) and scaled ratios  $S(N)$  (top) for Li, Be, B, C isotopes from the fragmentation of  $^{124}\text{Sn}$  and  $^{107}\text{Sn}$  projectiles at 600 A MeV (ALADIN) as a function of the neutron number  $N$ . The full line in the top panel represents the exponential fit curve  $C' \cdot \exp(\alpha N)$ . For clarity, some of the data symbols are slightly displaced horizontally.

Right panels: Scaled isotopic ratios  $S(N)$  for  $^{12}\text{C} + ^{112,124}\text{Sn}$  at  $E/A = 300$  and 600 MeV (INDRA) for three intervals of reduced impact parameter with "central" indicating  $b/b_{\text{max}} \leq 0.4$  and with offset factors of multiples of three. H, He, Li, Be and B fragments are distinguished by different data symbols as indicated. The dashed lines are the results of exponential fits according to Eq. (1). Only statistical errors are displayed (from ref. [34]).

The scaling expression

$$R_{21}(N, Z) = Y_2(N, Z)/Y_1(N, Z) = C \cdot \exp(\alpha N + \beta Z) \quad (1)$$

describes rather well the measured ratios over a wide range of complex particles and light fragments [31]. For illustration, the yield ratios  $R(124/107)$  obtained for the fragmentation of the  $^{124}\text{Sn}$  and  $^{107}\text{Sn}$  projectiles in the  $Z_{\text{bound}} = 10\text{-}30$  interval, covering the region of maximum fragment production, are plotted in Fig. 4 (bottom left). A fairly regular pattern can be recognized, the yield ratios for a given element increase with  $N$  and the lines of different elements are evenly displaced from each other. Fitting with the expression given above yields the parameters  $\alpha = 0.448$  and  $\beta = -0.503$  as indicated in the figure. The quality with which the isoscaling relation is obeyed is more easily judged for the scaled isotopic ratios  $S(N) = R_{21}(N, Z)/\exp(\beta Z)$  from which the  $Z$  dependence has been removed (Fig. 4, top panel).

Within the statistical model, there is a simple physical explanation for the appearance of isoscaling in finite systems. Charge distributions of fragments with fixed mass numbers  $A$ ,

as well as mass distributions for fixed  $Z$ , are approximately Gaussian with average values and variances which are connected with the temperature, the symmetry-term coefficient, and other parameters. The mean values depend on the total mass and charge of the systems, e.g. via the chemical potentials in the grand-canonical approximation, while the variances depend mainly on the physical conditions reached, the temperature, the density and possibly other variables. For example, the charge variance  $\sigma_Z \approx \sqrt{(AT/8\gamma)}$  obtained for fragments with a given mass number  $A$  in ref. [32] is only a function of the temperature and of the symmetry-term coefficient  $\gamma$  [33] since the Coulomb contribution is very small. This relation of isoscaling with the symmetry energy has attracted considerable interest recently.

## 6. THE SYMMETRY ENERGY

The dependence of  $S(N)$  on the impact parameter for the reactions  $^{12}\text{C} + ^{112,124}\text{Sn}$  at 300 and 600 MeV per nucleon, studied with INDRA at GSI [34], is shown in the right panels of Fig. 4. The slope parameter  $\alpha$  decreases strongly with increasing centrality to values smaller than 50% of those obtained for the peripheral event groups. In the grand-canonical approximation, assuming that the temperature  $T$  is about the same, the scaling parameters  $\alpha$  and  $\beta$  are given by the differences of the neutron and proton chemical potentials for the two systems divided by the temperature,  $\alpha = \Delta\mu_n/T$  and  $\beta = \Delta\mu_p/T$ . A proportionality of  $\alpha$  and  $1/T$ , with  $T$  derived from double isotope ratios, has been observed for light-ion (p, d,  $\alpha$ ) induced reactions at bombarding energies in the GeV range [28]. These data were, however, inclusive and thus not representative for multi-fragment decays because the mean fragment multiplicities are known to be small in this case [35].

The  $^{12}\text{C}$  induced reactions cover the rise of fragment production over the full range up to  $Z_{\text{bound}} \approx Z_{\text{proj}}/2$  with multiple fragment production being dominant in central collisions [21]. The measured temperatures rise slightly with centrality (note their similarity for the two systems) but not sufficiently fast in order to compensate for the decrease of the isoscaling parameter  $\alpha$  (Fig. 5, left panels), and  $\Delta\mu_n = \alpha \cdot T$  decreases according to the above relation.

The proportionality of  $\Delta\mu_n$  and thus of the isoscaling parameters with the coefficient  $\gamma$  of the symmetry-energy term  $E_{\text{sym}} = \gamma(A - 2Z)^2/A$  has been obtained from the statistical interpretation of isoscaling within the SMM [28] and Expanding-Emitting-Source Model [31] and confirmed by an analysis of reaction dynamics [36]. The relation is

$$\Delta\mu_n = \mu_{n,2} - \mu_{n,1} \approx 4\gamma\left(\frac{Z_1^2}{A_1^2} - \frac{Z_2^2}{A_2^2}\right) = 4\gamma\Delta(Z^2/A^2) \quad (2)$$

where  $Z_1, A_1$  and  $Z_2, A_2$  are the charges and mass numbers of the neutron-poor and neutron-rich systems, respectively, at breakup. The difference of the chemical potentials depends essentially only on the coefficient  $\gamma$  of the symmetry term and on the isotopic compositions. Using this equation and assuming that the isotopic compositions are practically equal to those of the original targets, an apparent symmetry-term coefficient  $\gamma_{\text{app}}$  was determined, i.e. without corrections for the effects of sequential decay. The results are found to be close to the normal-density coefficient  $\gamma \approx 25$  MeV for peripheral collisions but drop to lower values at central impact parameters (Fig. 5, bottom left).

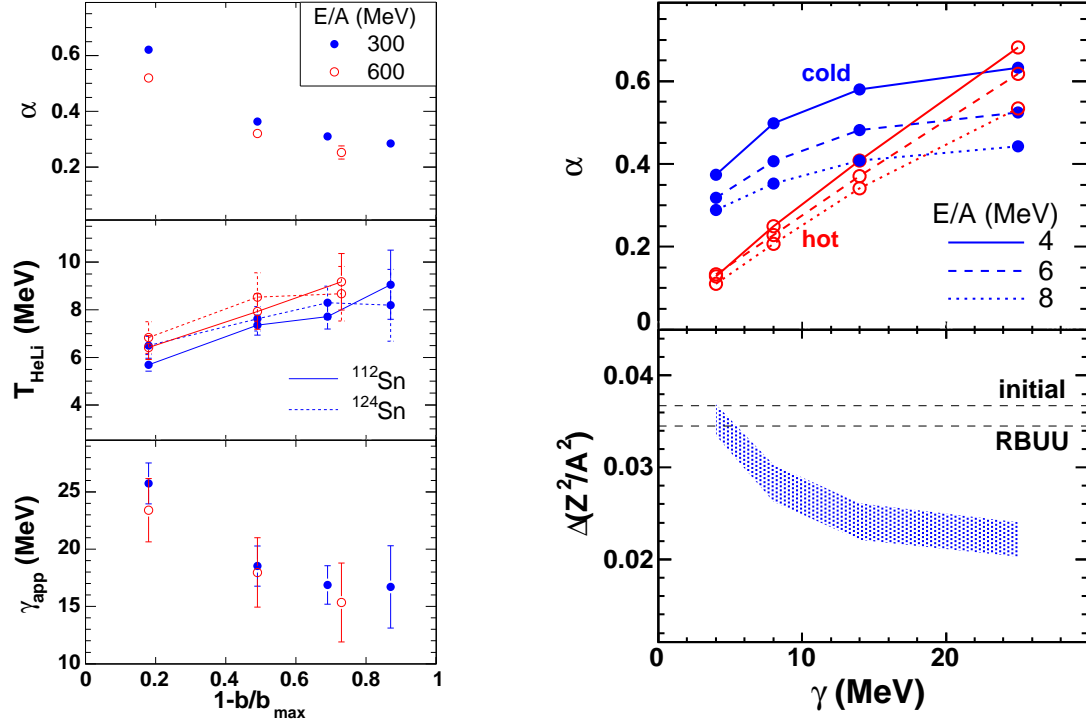


Figure 5. The left panels show the isoscaling coefficient  $\alpha$  (top), the double-isotope temperatures  $T_{\text{HeLi}}$  (middle) and the resulting  $\gamma_{\text{app}}$  (bottom) for the  $^{12}\text{C}$  on  $^{112,124}\text{Sn}$  reactions at  $E/A = 300$  MeV (full symbols) and 600 MeV (open symbols) as a function of the centrality parameter  $1 - b/b_{\max}$ .

The top right panel shows the isoscaling coefficient  $\alpha$  for hot (open circles) and cold fragments (dots) as a function of the symmetry-term coefficient  $\gamma$  as predicted by the Markov-chain calculations for  $^{112,124}\text{Sn}$  and excitation energies  $E/A = 4, 6, 8$  MeV. The shaded area in the bottom-right panel represents the region in the  $\Delta(Z^2/A^2)$ -versus- $\gamma$  plane that is consistent with the measured value  $\alpha = 0.29$  for central collisions and with the Markov-chain predictions for cold fragments. The dashed lines indicate the  $\Delta(Z^2/A^2) = 0.0367$  of  $^{112,124}\text{Sn}$  and the RBUU prediction (from ref. [34]).

The effects of sequential decay for the symmetry term, as calculated with the micro-canonical Markov-chain version of the SMM [37], are shown in the top-right panel of Fig. 5. Instead of using the above equations, the isoscaling coefficient  $\alpha$  was determined directly from the calculated fragment yields before (hot fragments) and after (cold fragments) the sequential-decay part of the code. The hot fragments exhibit the linear relation of  $\alpha$  with  $\gamma$  as expected but, for  $\gamma$  smaller than 25 MeV, the sequential decay causes a narrowing of the initially broad isotope distributions which leads to larger  $\alpha$  for the decay products. The variation of  $\alpha$  with  $\gamma$  is thus considerably reduced and the value  $\alpha < 0.3$  measured for the most central bins is only reproduced with input values  $\gamma \leq 10$  MeV, according to the calculations. Another possible source of uncertainty is the isotopic composition at breakup. Transport models predict that their difference for the two systems



should not deviate by more than a few percent from the original value [ 38] but larger deviations would have a significant effect as illustrated in Fig. 5, bottom right.

## 7. DISCUSSION

A decrease of the isoscaling parameter  $\alpha$  with increasing violence of the collision, beyond that expected from the simultaneous increase of the temperature, has also been observed for reactions at intermediate energy (refs. [ 41, 42] and references therein) and a systematics is emerging. A very recent interpretation of these results arrives at the conclusion that it is the reduced density rather than the elevated temperature which causes the symmetry term to be smaller than the standard value [ 43]. This analysis uses a temperature independent potential part of the symmetry term and a kinetic part in the form of a Fermi gas. Consequences of the low-density of the considered homogeneous system thus have to be assumed to be preserved in the process of fragment formation.

Statistical multifragmentation models as, e.g., the SMM [ 26] consider normal-density fragments statistically distributed within an expanded volume. Here a reduction of the symmetry term can be imagined to be caused by a modification of the fragments in the hot environment, including deformations or nuclear interactions between them. The neglect of such effects in the actual codes should probably be regarded as an idealization as the assumption of equilibrium at the final freeze-out stage requires interactions in order to achieve it. Fragment formation out of an expanded system can thus naturally explain variations of the symmetry term. The consequences for the predictions of this class of models are rather small since the partitioning is predominantly driven by the surface term in the liquid-drop description of the fragments while a variation of the symmetry term affects mainly the isotopic distributions [ 24, 39, 40].

Further studies will be needed in order to quantitatively establish the reduction of the symmetry term. The sequential decay corrections are obviously important but also the evolution of the isotopic compositions during the reaction process deserves attention. An experimental reconstruction of the neutron-to-proton ratio of the detected spectator systems seems possible with the data from the ALADIN experiments. The spectator source of neutrons required for this purpose has already been identified with the coincident data from the LAND neutron detector [ 44].

The fruitful collaboration and stimulating discussions with my colleagues S. Bianchin, A.S. Botvina, J. Brzychczyk, A. Le Fèvre, J. Łukasik, P. Pawłowski and C. Sfienti are gratefully acknowledged.

## REFERENCES

1. W. Trautmann, Nucl. Phys. A 752 (2005) 407c.
2. C. Sfienti et al., contribution to this conference.
3. for reviews see, e.g., Topical Volume on 'Dynamics and Thermodynamics with Nuclear Degrees of Freedom', edited by Ph. Chomaz et al., Eur. Phys. J. A (2006), in press.
4. J.M. Lattimer and M. Prakash, Phys. Rep. 333 (2000) 121.
5. A.S. Botvina and I.N. Mishustin, Phys. Lett. B 584 (2004) 233.
6. A.S. Botvina and I.N. Mishustin, Phys. Rev. C 72 (2005) 048801.
7. Bao-An Li, Phys. Rev. Lett. 88 (2002) 192701.

8. V. Greco et al., Phys. Lett. B 562 (2003) 215.
9. Gao-Chan Yong, Bao-An Li, Lie-Wen Chen, preprint nucl-th/0606003.
10. J. Pouthas et al., Nucl. Instr. Meth. in Phys. Res. A 357 (1995) 418.
11. W. Trautmann, in Proceedings of the Seventh International Conference on Nucleus-Nucleus Collisions, Strasbourg, France, July 2000, ed. by W. Nörenberg, D. Guerreau and V. Metag, Nucl. Phys. A 685 (2001) 233c.
12. H. Müller and B.D. Serot, Phys. Rev. C 52 (1995) 2072.
13. H. Jaqaman, A.Z. Mekjian, L. Zamick, Phys. Rev. C 27 (1983) 2782.
14. J. Schnack and H. Feldmeier, Phys. Lett. B 409 (1997) 6.
15. H. Xi et al., Z. Phys. A 359 (1997) 397; erratum in Eur. Phys. J. A 1 (1998) 235.
16. S. Fritz et al., Phys. Lett. B 461 (1999) 315.
17. J.B. Natowitz et al., Phys. Rev. C 65 (2002) 034618.
18. V.E. Viola, in Proceedings of the Eight International Conference on Nucleus-Nucleus Collisions, Moscow, Russia, June 2003, ed. by Yu. Oganessian and R. Kalpakchieva, Nucl. Phys. A 734 (2004) 487.
19. V.E. Viola et al., Phys. Rev. Lett. 93 (2004) 132701.
20. B. Tamain, in ref. [ 3], Eur. Phys. J. A (2006), in press.
21. A. Schüttauf et al., Nucl. Phys. A 607 (1996) 457.
22. C. Sfonti et al., Nucl. Phys. A 749 (2005) 83c.
23. M.V. Ricciardi et al., Nucl. Phys. A 733 (2004) 299.
24. N. Buyukcizmeci, R. Ogul, A.S. Botvina, Eur. Phys. J. A 25 (2005) 57.
25. P. Napolitani et al., Phys. Rev. C 70 (2004) 054607.
26. J.P. Bondorf et al., Phys. Rep. 257 (1995) 133.
27. M.B. Tsang et al., Phys. Rev. Lett. 86 (2001) 5023.
28. A.S. Botvina, O.V. Lozhkin, W. Trautmann, Phys. Rev. C 65 (2002) 044610.
29. G.A. Souliotis et al., Phys. Rev. C 68 (2003) 024605.
30. W.A. Friedman, Phys. Rev. C 69 (2004) 031601(R).
31. M.B. Tsang et al., Phys. Rev. C 64 (2001) 054615.
32. A.S. Botvina, A.S. Iljinov, I.N. Mishustin, Sov. J. Nucl. Phys. 42 (1985) 712.
33. the notation follows that originally chosen in Ref. [ 26]; alternatively  $C_{\text{sym}}$  is frequently used for the same quantity.
34. A. Le Fèvre et al., Phys. Rev. Lett. 94 (2005) 162701.
35. L. Beaulieu et al., Phys. Lett. B 463 (1999) 159 and Phys. Rev. Lett. 84 (2000) 5971.
36. A. Ono et al., Phys. Rev. C 68 (2003) 051601(R).
37. A.S. Botvina and I.N. Mishustin, Phys. Rev. C 63 (2001) 061601(R).
38. T. Gaitanos et al., Nucl. Phys. A 732 (2004) 24 and private communication.
39. R. Ogul and A.S. Botvina, Phys. Rev. C 66 (2002) 051601.
40. A.S. Botvina et al., preprint nucl-th/0606060, Phys. Rev. C in press.
41. D.V. Shetty et al., Phys. Rev. C 71 (2005) 024602.
42. G.A. Souliotis et al., Phys. Rev. C 73 (2006) 024606.
43. Bao-An Li and Lie-Wen Chen, preprint nucl-th/0605002.
44. W. Trautmann et al., in Proceedings of the IWM2005 International Workshop on Multifragmentation and related topics, Catania, Italy, 2005, edited by R. Bougault et al., Conf. Proc., Vol. 91 (Italian Physical Society, Bologna, 2006) p. 157; preprint nucl-ex/0603027.